26

Omni-directional Mobile Microrobots on a Millimeter Scale for a Microassembly System

Zhenbo Li, Jiapin Chen
Shanghai Jiao Tong University
P.R. China

1. Introduction

The development of microrobots on a millimeter scale has recently received much attention. The environments in which these robots are supposed to operate are narrow and potentially complicated spaces, such as micro-factory, blood vessel, and micro-satellite. The robots must have omni-directional mobility, high power and high load capacity, within a scale in millimeters, in order to accomplish the work efficiently.

Motion principles and actuation mechanisms that combine volume, motion of resolution, and the speed virtues of coarse positioning, are still the challege in the microrobot design. Different principles to drive microrobots have been developed. The Microprocessor and Interface Lab of EPEL developed a 1cm^3 car-like microrobot with two Smoovy 3 mm motors. Sandia National Lab developed a 4cm^3 volume and 28g weight microrobot for plume tracking with two Smoovy micromotors with a car-like steering (Byrne et al., 2002). AI lab in MIT designed Ants microrobot with a 36.75cm^3 volume and 33g weight, driven like a tank with pedrail (Mclurkin, 1996). Caprari and Balmer built another car-like microrobot with 8cm^3 volume by watch motor (Caprari et al., 1998). Dario developed a millimeter size microrobot by a novel type of electromagnetic wobble micromotor, with a three-wheel structure (Dario et al., 1998). Besides the normal motors driven principle, other microactuation techniques based on smart materials have been devised, such as piezoelectric actuators, shape memory alloys, etc. The MINIMAN robot and the MiCRoN microrobot have employed these techniques (Schmoeckel & Fatikow, 2000; Brufau et al., 2005). The first walking batch fabricated silicon microrobot, with the 15x5 mm^2 size, able to carry loads has been developed and investigated. The robot consists of arrays of movable robust silicon legs having a length of 0.5 or 1 mm. Motion is obtained by thermal actuation of robust polyimide joint actuators using electrical heating (Thorbjörn et al., 1999).

Omni-directional mobile robots have kept developing due to inherent agility benefits (Williams et al., 2002). The mechanisms can be divided into two approaches: special wheel designs and conventional wheel designs. Fujisawa et al., Ferriere and Raucent developed the universal wheel for omni-directional mobility (Fujisawa et al., 1997; Ferriere et al., 1998). Muri and Neuman developed the Mecanum wheel similar to the universal one (Muir & Neuman, 1987). West and Asada developed the ball wheel (West & Asada, 1997), while Killough and Pin developed the orthogonal wheel (Killough & Pin, 1994).

Source: Mobile Robots Towards New Applications, ISBN 3-86611-314-5, Edited by Aleksandar Lazinica, pp. 784, ARS/plV, Germany, December 2006

These special wheel designs have demonstrated good omni-directional mobility; however, they generally require complex mechanical structures. Other researchers have tried to develop the omni-directional vehicle by conventional wheels. Boreinstein, et al, designed the omni-directional structure using steered wheels (Boreinstein et al, 1996), while Wada and Mori used active castor wheel (Wada & Mori, 1996). Mobile microrobot and omni-directional mobile robot have been well developed recently (Kim et al., 2003). However, few omni-directional mobile microrobot have been reported. Specially-developed wheels are very difficult to realize on millimeters scale due to their complexity. Furthermore, these structures have limited load capacity with slender rollers. Conventional wheels are the feasible solution for omni-directional mobile microrobot within $1cm^3$ volume, due to their inherent simple structure. However, the microactuator within 10 mm^3 with high power output is still a challenge at present.

This paper aims to present such an omni-directional mobile microrobot within the volume of $1cm^3$ for microassembly. Microassembly is one chief application for mobile microrobots. Most reported mobile microrobots for micro assembly are based on piezoelectricity actuators to meet the high requirement of position precision. However, the piezoelectricity actuators usually suffer from complex power units that are expensive and cumbersome and which do not easily allow for wireless operation. Furthermore, piezoelectric actuators are complex systems that exhibit non-linear behavior and as a result they lack an accurate mathematical model that can provide a reliable prediction of the system's behavior (Vartholomeos, 2006). This chapter aims to present the construction of an omni-directional mobile microrobot system, with the microrobot less than $1cm^3$ volume and its unique dual-wheels driven by electromagnetic micromotors in a 2mm diameter for purpose of microassembly in narrow space. The design, fabrication, kinematics analysis, and control of microactuators and microrobots, are to be discussed with details of the sub-areas.

2. Design of omni-directional microrobots on a millimeter scale

Like macrorobots, microrobots are composed of electromechanical systems, mainly chassis planes and wheels units. In this section, the construction of omni-directional microrobots on a millimeter scale, the design of novel dual-wheel structure for microrobots and axial flux electromagnetic micromotors for dual-wheels, and fabrication of the stator winding for micromotors are to be described in sub-sections.

2.1 Structure of omni-directional microrobots

Two generations of omni-directional mobile microrobots, OMMR-I and OMMR-II, as shown in Fig. 1 and Fig. 2, have currently been developed. OMMR-I, on a scale of 8mm×8mm×6mm, is constructed with two dual-wheels; while OMMR-II with three dual-wheels, is with scales in 9.8mm×9.8mm×6mm.

The omni-directional microrobots consist of two or three novel designed dual-wheels, to be described in Section 2.2. These dual-wheels, connected with each other by a set of gears and driven by specially-designed electromagnetic micromotors, to be described in Section 2.3, are evenly distributed on the chassis plane. The set of gears are fabricated by LIGA (Lithographie GalVanoformung Abformung) process, with a gear ratio of 1:3. Each dual-wheel structure needs one separate micromotor to produce the translation movement, meanwhile, the rotation movement of all dual-wheel structures is produced by one single micromotor.

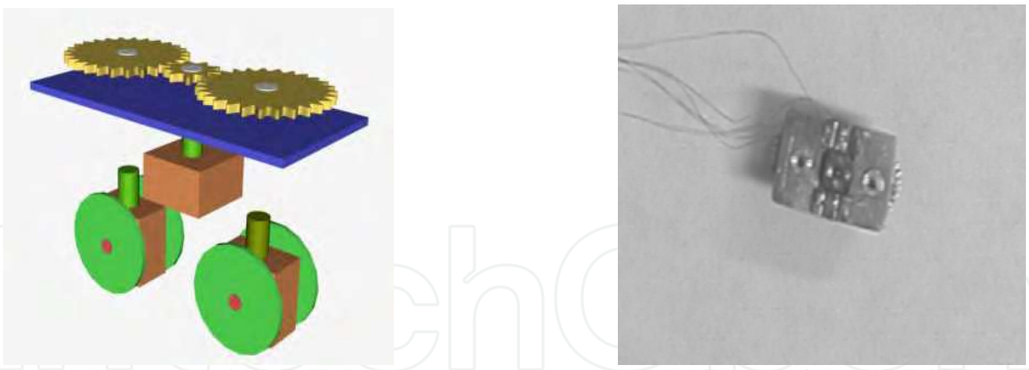

(a) Structure of OMMR-I (b) Photo of the OMMR-I

Fig. 1. Structures and photos of the omni-directional microrobot-I (OMMRI).

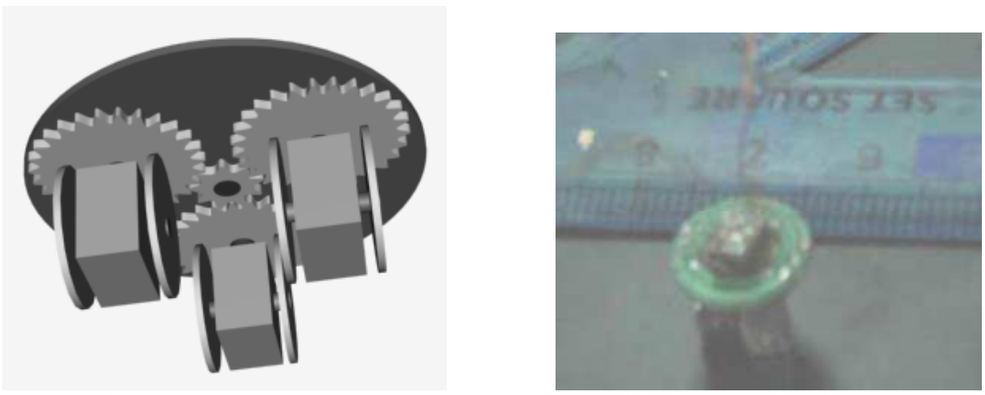

(a) Structure of OMMR-II (b) Photo of the OMMR-II

Fig. 2. Structures and photos of the omni-directional microrobot-II (OMMRII).

All translation micromotors are controlled as one motor, to rotate synchronously. The active gear, in the middle of the chassis, is driven by steering micromotor, and the passive gears are connected to dual-wheel structures through an axis perpendicular to the chassis plane. Power from the steering micormotor is transmitted through gears to the axis, and then to the dual-wheels via friction between the wheels and ground. Therefore, all dual-wheel structures keep the same direction at any moment. Moreover, this set of microgears can also amplify rotary driving power and improve the rotary positioning accuracy of microrobots.

2.2 Design of novel duel-wheel structure

Conventional wheels for omni-directional mobile robots can generally be divided into three types, centred wheels, offset wheels, and dual-wheels, as shown in Fig. 3. Mobile robots with centred wheels must overcome dry-friction torque when reorienting the mobile robots because of the fixed wheels, however, mobile robots with dual wheels, kinematically equivalent to centred wheels, only need to overcome rolling friction. Moreover, compared with robots with offset wheels of identical wheels and actuators, robots with dual-wheel structure can double the load-carrying ability by distributing the load equally over two wheels. However, the complexity of an omni-directional mobile robot with a conventional dual-wheel structure can not be applied into microrobots with scales in millimeters. Therefore, a new dual-wheel structure is required to be designed for an omni-directional microrobot on a millimeter scale for a microassembly system.

(a) centred wheel (b) offset wheel (c) dual wheel

Fig. 3. Structure of the three types of conventional wheels.

This novel duel-wheel structure, as shown in Fig. 4, is composed of two traditional coaxial wheels, separated at a distance and driven by a electromagnetic micromotor, to be described in Section 2.3. The characteristic of this design is that dual-wheels are driven by only one motor and by frictional forces independently, instead of the two motors. The goal of this design is to keep the volume of microrobots within $1cm^3$ through simplifying the structure of micromotors; meanwhile, mircorobots can have omni-directional mobility, high load capacity and positioning accuracy.

This novel dual-wheel structure has certain advantages over single-wheel designs and conventional dual-wheels. Single-wheel structures produce relatively high friction and scrubbing when the wheel is actively twisted around a vertical axis. This will cause slip motion, therefore, reducing the positioning accuracy and increasing the power consumption, a crucial parameter for a microrobot. The scrubbing problem can be reduced by using dual-wheels. However, in ordinary dual-wheel structures, both wheels are driven by two independent motors, which will increase the complexity of the construct and the size of the structure for a microrobot. This new structure can change the dry-friction between the dual-wheels and the ground into rolling resistance during its steering and keep the small volume of microrobots as well. Two coaxial wheels, namely, active wheel and passive wheel, are connected to one micromotor shaft on both sides. The active wheel is fixed to the shaft driven by the micromotor; meanwhile, the passive wheel has rotary freedom around the shaft, driven by frictional forces between itself and the ground. Friction during translation leads to the active wheel and the passive wheel rotating synchronously, however, the two wheels rotate in opposite directions during steering. Therefore, omni-directional mobility with reduced wheel scrubbing on a millimeter scale is produced by this dual-wheel structure design.

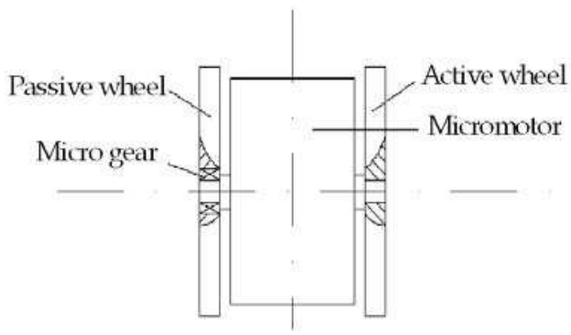

Fig. 4. Structure of novel dual-wheel.

2.3 Design of axial flux electromagnetic micromotor

Actuators are a crucial part in designing microrobots, mainly because of the lack of currently available micromotors and the unsatisfying performance of existing ones. Forces, such as

electrostatics, piezoelectricity hydraulics, pneumatics, and biological forces, scale well into the micro domain, but some of them are difficult to be built in millimeters' size. Electromagnetic forces can give micromotors larger output torque (Fearing, 1998) and longer operating lifetime than others in the same volume. Electromagnetic micromotors, such as smoovy micromotors and IMM (Institut für Mikrotechnik Mainz GmbH) micromotors, are designed with radius flux structure. However, the height of micromotors is several times larger than the diameter. Therefore, in this section, an original axial flux electromagnetic micromotor, as shown in Fig. 5, is designed with the following characteristics:

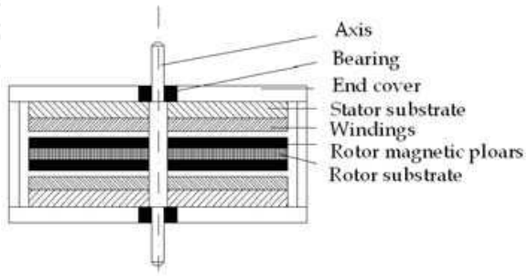

Fig. 5. Structure of the 2mm micromotor.

- the axial magnetic field shrinking the volume of micromotor
- a novel structure consisting of one rotor set between two stators
- the rotor having multipolar permanent magnets with high performance
- the stators having slotless concentrated multilayer planar windings

2.3.1 Structure and analysis

Electromagnetic micromotors, according to directions of magnetic flux, can be divided into two types, radial flux and axial flux micromotors, as shown in Fig. 6. Comparing with radial flux micromotors, axial flux ones can improve the efficiency of electromagnetic energy transformation, and enlarge the electromagnetic interaction area between a rotor and a stator, the most important parameter for a micromotor. An electromagnetic micromotor with a magnetic flux 'sandwich' structure---two stators in outliers and one rotor inside---for enough torque output is designed shown in Fig. 5.

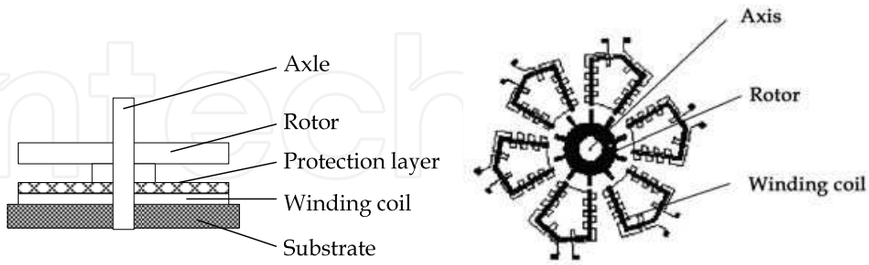

a. The structure of axial magnetic field b. The structure of radial magnetic field

Fig. 6. The structure of electromagnetic micromotor.

According to the principle of $T = BILr$, the torque output (T), a critical measuring parameter for micromotors, is directly proportional to the magnetic flux density in the gap (B), current value of winding (I), valid winding length (L), and spinning radius (r). Although the design of multilayer windings has been adapted to increase the valid winding length, the overall micro size of micromotors limits values of L and r. Hence, the magnetic flux intensity becomes the key factor in

improving the performance of the micromotor. The selection of magnetism materials with high properties and the design of an optimum magnetic circuit become key factors to improve torque output. In current research, the stator winding has been designed in slotless and multiple layers, therefore, the air gap in the electromagnetic micromotor can include the height of the stator winding itself. This results in a difference in the magnetic flux density between the winding layers. The relationship between the flux strength and the air gap width is shown in Fig. 7.

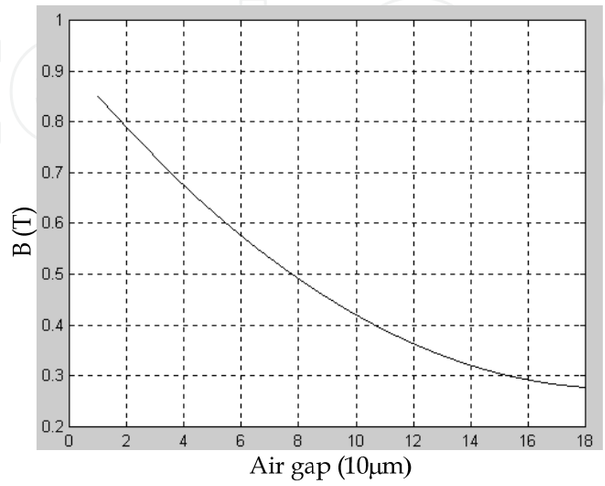

Fig. 7. Relationship between magnetic flux density and air gap.

The attractive force, in the z direction between the rotor and the stator, increases sharply as the gap (g) decreases. When g is 0.05mm, the attractive force reaches 27.7mN, one thousand times larger than the weight of the rotor (<2mg). Therefore, the friction force caused by the attractive force will be much larger than that caused by the weight of the rotor.

2.3.2 Optimal design of micromotor parameters with genetic algorithms (GA)

2.3.2.1 Targets of the design

Performance indices, such as efficiency, torque output, speed, and operating lifetime, can be used to measure a motor. Two of them are selected as main targets in this design:

- larger torque output
- less loss of power

The torque output is a key index evaluating the performance of a motor. The heating loss of the windings is the main loss of power in micromotors. It will affect the operating lifetime of micromotors. Although the absolute value of this loss is not large, it is still crucial to the operating lifetime of electromagnetic micromotors because of the overall micro size and the high intensity of power. Therefore, the less loss of heating power is defined as another target of the design.

2.3.2.1 Mathematical model of the micromotor

Having selected the targets of this design, with the purpose of applying genetic algorithms (GA) into this design, the mathematical models of electromagnetic micromotors has been drawn as follows:

$$T = \sum_{i=1}^{m}\sum_{j=1}^{n} B_i I L_j r \eta \tag{1}$$

$$P_H = I^2 R \tag{2}$$

$$R = \sum_{j=1}^{m}\sum_{i=1}^{n} \rho l_i / S \tag{3}$$

$$S = bh \tag{4}$$

$$E = \sum_{i=1}^{m}\sum_{j=1}^{n} B_i \frac{2\pi N}{60} r L_j \tag{5}$$

T is the torque output of single phase
m is the number of the layer of the stator
n is the number of the turn of the winding
B_i is the magnetic flux density of the i^{th} layer of the stator
I is the value of rated current
L_j is the average effective length of a coil in a phase of winding
r is the average radius of the circle track of the centroid of effective winding
η is the compromise coefficient
P_H is the loss of heating of single phase
R is the value of resistance of single phase winding
ρ is the conductive coefficient of copper
l_i is the length of a circle in single phase winding
S is the area of the wire in winding
b is the width of the wire in winding
h is the height of the wire in winding
E is the back EMF of single phase
N is the speed of the motor ;

The above formulas show that larger output and less heating loss are a constraint satisfaction problem (CSP) (Li & Zhang, 2000). Larger torque output can be obtained through either increasing layer numbers of the stator or loop numbers of the winding, however, both of them will lead to more heating loss. Meanwhile, the increase in the layers of the stator will result in a larger air gap, corresponding to smaller values of magnetic flux density. Likewise, the torque output will drop when decreasing the heating loss. The solutions to the constraint satisfaction problem are to be discussed in the following subsections.

2.3.2.2 Application of GA in the micromotor design

- **Definition of objective function**

The application of GA in this design is put forth to solve the CPS in the design of the micromotor. As the only dynamic factor to guide the search of GA, the value of objective function, φ, directly affects the efficiency and result of algorithms. The objective function should combine with specific design targets for its reasonability in physics. Therefore, in this design of the micromotor, the power of the micromotor has been selected as a bridge to combine the torque output and the heating loss. Through changing coefficients, different

parameters can be reached to satisfy various applications of the micromotor. The objective function in physics can be described as follows:

$$\varphi = \lambda(TN/9550) - \mu\left(I^2 R\right) \tag{6}$$

Because of the low efficiency of micromotors, the objective function will not keep positive value in its domain, which will result in the low efficiency of the algorithm. Hence, in this research, it is not suitable for the search to value the objective function from the limitation of GA. A basic positive constant is required to be added to make the signature of φ positive during the search without changing the physical meaning of φ. Another issue, to be considered, is that the number of design variables is not unique. The large domain of each variable, leading to the large domain of the objective function, will bring negative effect to the search of GA. Therefore, the space of objective function has been compressed by using the mathematical method, logarithm, keeping the signification of objective function.

$$\varphi = \ln\left(BASE + \lambda(TN/9550) + \mu\left(I^2 R\right)\right) \tag{7}$$

- **Definition of variables**

From the formulas (1) and (2), it can be seen that the constraint satisfaction problem (CSP) between torque output and heating loss is embodied in parameter contradictions of the layer number, the circle number and the height of the stator winding. As a result, the three parameters are defined as the variables in the design of the micromotor.

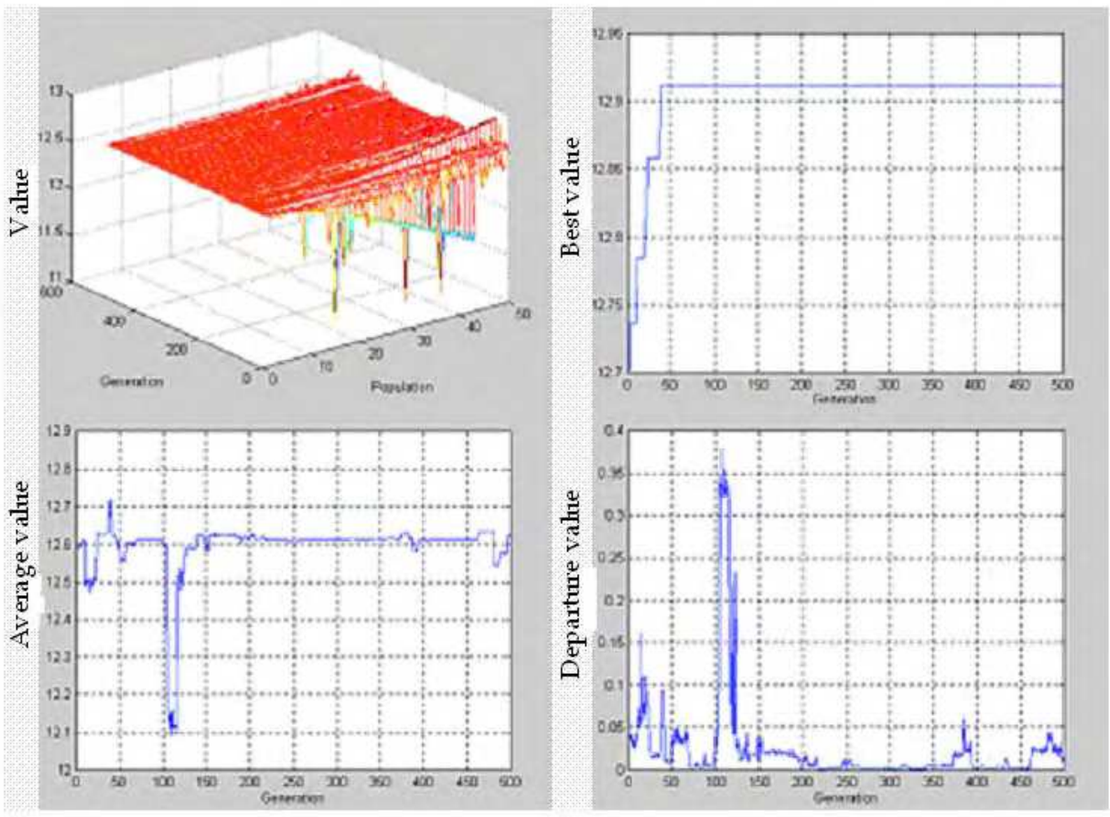

Fig. 8. The curves expressing the application of GA in the design of micro-motor.

The search space of each variable is defined by combining its physical meaning and the constraints fo micromanufacture as following:

$$\theta = [m, n, h]$$

m∈[1 , 8] ; n∈[1 , 14] ; h∈ (0.0 , 16.0)

The search state space is shown in the first chart of Fig. 8. Other charts in Fig. 8 show the average value of the fitness, the best value of the fitness, and the departure value of the fitness of each generation, respectively.

The best solution obtained by the application of GA is shown as following:

m=4, n=9, H=14.24mm

2.4 Fabrication process of the stator winding

According to the results of optimal design with GA, a stator winding of the electromagnetic micromotor in a diameter of 2mm is manufactured by microfabrication technique. The stator winding, composed of 4 layers of coils, 54 turns, and 3 pairs, is only 2mm in diameter and 1μm in minimum line space with the maximum operation current of the coils of 230mA and resistor is 22-30Ω. The structure of the winding is shown as Fig. 9.

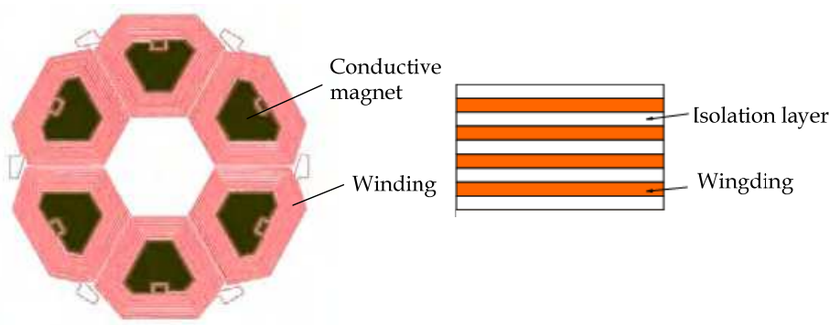

(a) Top view Figure (b) Section Figure

Fig. 9. Structure of the structure.

The substrate is a special ferrite wafer, 4mm in thickness and 3-inch-diameter. In total 13 masks are required during the winding process of the stator, and coils and connectors are fabricated by mask-plating process (Zhao et al. 1999). 4 layers of alumina isolation layers are deposited by a sputter machine. The basic processes of the stator winding are described as follows, and the flow charts are shown in Fig. 10.

1. Depositing a seed-layer (Cu/Cr or Cu/Ti) with 100nm thickness on the ferrite substrate for the electro-plating by sputter process. Cu is the electrode for electroplating, while the Cr or Ti is used to increase the adherence force between the seed-layer and substrate. The processes are shown in Fig. 10(a, b).
2. Spin-coating a photoresist layer, which is patterned to form the mask for electro-plating the windings after the exposure and developing processes, shown in Fig. 10 (c, d)
3. Electro-plating from the seed layer to form the windings with designed structure, shown in Fig. 10 (e)
4. Spin-coating the second photoresist layer, which is patterned to form the mask for electro-plating the connecting wire between the two adjacent windings layers, after the exposure and developing processes, shown in Fig. 10 (f, g)

5. Electro-plating to form the connectors between the two adjacent layers windings, shown in Fig. 10 (h)
6. Removing the photoresist layer by actone, shown in Fig. 10 (i)
7. Removing the seed-layer by sputter etching process, shown in Fig. 10 (i)
8. Depositing an insulation layer (alumina) by sputter process, shown in Fig. 10 (j).
9. Removing the unwanted part of the insulation to bare the connectors between the two layers by lapping and polishing, shown in Fig. 10 (k)
10. Fabricating the second winding layer by repeat the above steps.

The fabrication difficulty of the stator increases with the increasing of the number of winding layers. Structure design of the micromotors for microrobot of this project select a 4-layer structure according to the results of the optimal design with GA. The structure of the stator is shown in Fig. 11.

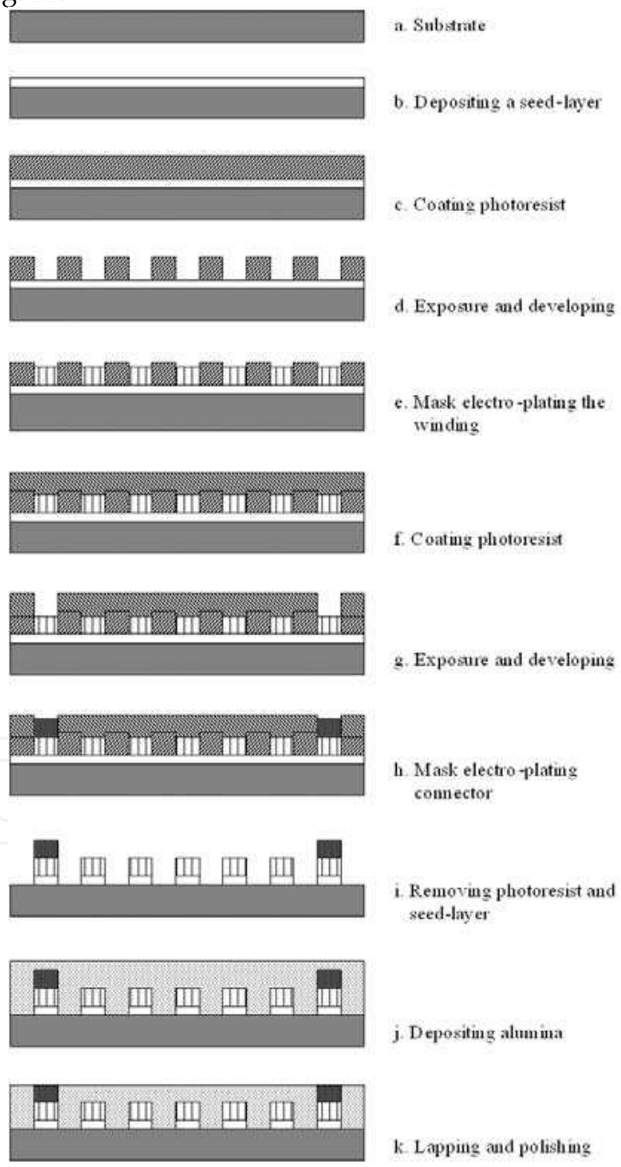

Fig. 10. Fabrication process of the stator winding.

Fig. 11. Photo of the stator.

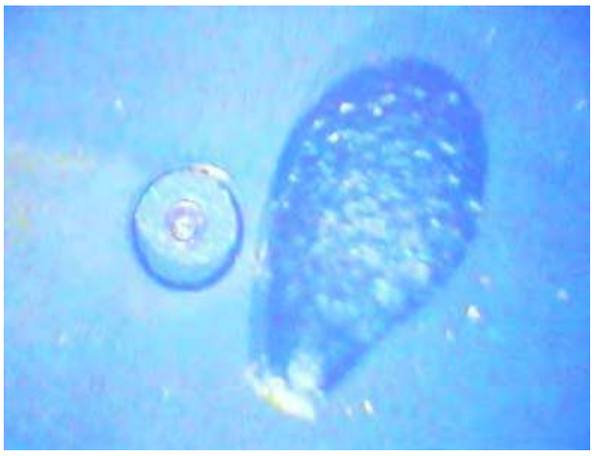

Fig. 12. Photo of the micromotor and a sesame seed.

The rotor is made from SmCo permanent magnetic alloy. A special magnetization method has been developed to write pairs of magnetic poles on the surface of rotor in the vertical direction. The photo of the micromotor in contrast to the sesame is shown in Fig. 12, and its performance is shown in Table 1.

Over size (mm)	Max speed (rpm)	Weight (mg)	Range of timing	Max torque output (μNm)
2.1×2.1×1.3	28000	38	50:1	2.8

Table 1. Main performance parameter of the micromotor.

3. Kinematics characteristics of the omni-directional microrobot

The structure of the novel duel-wheels has been described in previous section of this chapter. The active wheel is fixed to the micromotor shaft, while the passive wheel has the rotary freedom around the shaft. When the duel-wheel turns, the vertical shaft (transmission gear shaft) doesn't move. Therefore we can simplify the complicated wheels as a single virtual wheel locating in the center of the duel-wheel with zero thickness, which is drawn as the broken line in Fig. 13. In the coordinate systems defined in Fig. 13,

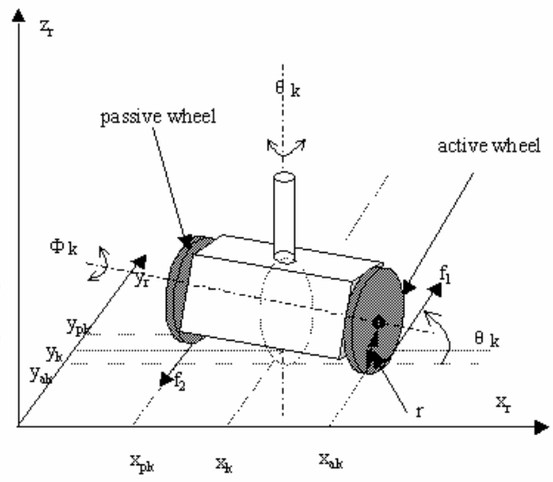

Fig. 13. Coordinate systems of a dual-wheel.

$C_r = (O_r, X_r, Y_r, Z_r)$ is the robot inertial coordinate frame

$C_0 = (O_0, X_0, Y_0, Z_0)$ is the ground inertial coordinate frame

ψ the angle which C_r offset C_0

x_{ak} x Coordinate of the point the Kth active wheel contacting with ground

y_{ak} y Coordinate of the point the Kth active wheel contacting with ground

x_{pk} x Coordinate of the point the Kth passive wheel contacting with ground

y_{pk} y Coordinate of the point the Kth passive wheel contacting with ground

x_k x Coordinate of the point the Kth virtual wheel contacting with ground

y_k y Coordinate of the point the Kth virtual wheel contacting with ground

$\theta_k(t)$ Rotation angle of the Kth virtual wheel from the vertical axis at time T

$\phi_k(t)$ Rotation angle of the first virtual wheel from the horizontal axis at time T

Since the microrobot moves on a plane, the coordinate C_r is chosen to satisfy the analytical requirement. Therefore, the pose vector ξ consists of the Descartes coordinate of the reference point O_r in coordinate C_0 and the offset angle C_r from C_0. Because the microrobot carried by the duel-wheels moves on a plane, its motion has three degrees of freedom. Where the microrobot consists of n (n=2, 3) duel-wheel structures, the microrobot state (s) can be expressed with 3+2×n vectors (Alexander, 1989):

$S=[\xi\ \theta\ \phi]^T$

Where,

$\theta=[\theta_1\ \theta_2\ \ldots\theta_n]^T$

and

$\phi=[\phi_1\ \phi_2\ \ldots\phi_n]^T$.

3.1. Kinematics constraints of the microrobot wheel

While the microrobot moves, the wheels only roll on the plane without slip. The velocity of the contact point between the virtual wheel and the ground is zero.

$$-\dot{x}\cdot\sin(\psi+\theta_k)+\dot{y}\cdot\cos(\psi+\theta_k)+(x_k\cdot\cos\theta_k+y_k\cdot\sin\theta_k)\dot{\psi}=0 \tag{8}$$

$$\dot{x}\cdot\cos(\psi+\theta_k)+\dot{y}\cdot\sin(\psi+\theta_k)+(x_k\cdot\sin\theta_k-y_k\cdot\cos\theta_k)\dot{\psi}-r_k\cdot\dot{\phi}_k=0 \tag{9}$$

Therefore, the steering motion of the microrobot and the angular velocity of the virtual wheel can be drawn as following:

$$\theta_k=Arctg\frac{-\dot{x}\cdot\sin\psi+\dot{y}\cdot\cos\psi+x_k\cdot\dot{\psi}}{\dot{x}\cdot\cos\psi+\dot{y}\cdot\sin\psi-y_k\cdot\dot{\psi}} \tag{10}$$

$$\dot{\phi}_k=\frac{\dot{x}\cdot\cos(\psi+\theta_k)+\dot{y}\cdot\sin(\psi+\theta_k)}{r_k}+\frac{(x_k\cdot\sin\theta_k-y_k\cdot\cos\theta_k)\dot{\psi}}{r_k} \tag{11}$$

The microrobot kinematics constraints can be expressed by considering the n duel-wheels.

$$K(\underline{\theta})\cdot R(\psi)\cdot\dot{\xi}=0 \tag{12}$$

$$J_1(\underline{\theta})\cdot R(\psi)\cdot\dot{\zeta}-J_2\dot{\phi}=0 \tag{13}$$

where

$$K(\underline{\theta})=\begin{pmatrix}-\sin\theta_1 & \cos\theta_1 & x_1\cdot\cos\theta_1+y_1\cdot\sin\theta_1\\ -\sin\theta_2 & \cos\theta_2 & x_2\cdot\cos\theta_2+y_2\cdot\sin\theta_2\\ \vdots & \vdots & \vdots\\ -\sin\theta_n & \cos\theta_n & x_n\cdot\cos\theta_n+y_n\cdot\sin\theta_n\end{pmatrix} \tag{14}$$

$$J_1(\underline{\theta})=\begin{pmatrix}\cos\theta_1 & \cos\theta_1 & x_1\cdot\sin\theta_1+y_1\cdot\cos\theta_1\\ \cos\theta_2 & \cos\theta_2 & x_2\cdot\sin\theta_2+y_2\cdot\cos\theta_2\\ \vdots & \vdots & \vdots\\ \cos\theta_n & \cos\theta_n & x_n\cdot\sin\theta_n+y_n\cdot\cos\theta_n\end{pmatrix} \tag{15}$$

$$J_2=\begin{pmatrix}r_1 & 0 & 0 & 0\\ 0 & r_2 & 0 & 0\\ 0 & 0 & \ddots & 0\\ 0 & 0 & 0 & r_n\end{pmatrix} \tag{16}$$

Assuming A(s) expresses the constraints matrix of microrobot kinematics,

$$A(s)=\begin{pmatrix}K(\underline{\theta})\cdot R(\psi) & 0 & 0\\ J_1(\underline{\theta})\cdot R(\psi) & 0 & -J_2\end{pmatrix} \tag{17}$$

then the kinematics constraint equation is

$$A(\underline{s})\cdot\dot{\underline{s}}=0 \tag{18}$$

3.2. Kinematics analysis of the omni-direction microrobot

The kinematics of the omni-directional microrobot is used to analyze the possible mobility under the kinematics constraint equation (11).

1) The Mobility

From the equation (12), the state vector $R^t(\psi)\cdot\dot{\xi}$ belongs to the zero space of matrix $K(\underline{\theta})$. This produces the movement constraint of the microrobot, while the equation (13) doesn't constrain

.

the movement. The condition can be satisfied by giving the vector $\dot{\underline{\phi}}$ a suitable value:

$$\dot{\underline{\phi}} = J^{-1} \cdot J_1(\underline{\theta}) \cdot R(\psi) \cdot \dot{\zeta} \tag{19}$$

Therefore, the zero space of is only to be considered to study the mobility of microrobot. $K(\underline{\theta})$

When the turning angle the microrobot is fixed, the matrix is n×3 because the microrobot has n duel-wheels. When $n \geq 3$, the matrix order is 3 normally, which means the robot has good mobility on a plane. However, as n=2, the matrix order is 2 normally, which means its order is equal to 1 only when the head direction of the microrobot is perpendicular to the connecting line of the two castor centre points. Therefore, the velocity vector of the microrobot is a one-dimension space except that the special situation ξ is a two-dimension space. This is solved by adding two supporting points in the design. Thus, the microrobot is proved to have only one freedom when it moves around the plane.

2) The Directionality

Under the constraint of equation (12), the directionality is defined to the microrobot movement when the vector $\underline{\theta}$ changes with time.

The angle of the microrobot to the frame $\underline{\theta}$, can be obtained by the following equation, while the state of the microrobot and the velocity vector at this moment are known:

$$K(\theta) \cdot R^t(\psi) \cdot \underline{v} = 0 \tag{20}$$

It proves that the microrobot can achieve omni-directional mobility under the kinematics constraint of equation (12).

4. Control of the omni-directional microrobot

The 2mm micromotor, with the 8-polar rotor and the 9-coil stator, has been designed as a 3-phase synchronous motor in the star-connected windings. Controlled with 2-2 phases conduct approach (2-2 PCA) and 3-3 phases conduct approach (3-3 PCA), micromotors can work as a synchronous motor with different speeds (reference 10). 2-2 PCA means two phases conduct current at any time and leave the third floating, whose vector figure is shown in Fig. 14(a). $A\bar{B}$ represents that current in windings is from A to B via the middle point. 3-3 PCA means all the three phases are conducted. $A\bar{B}C$ represents that current in windings is from both A and C to B via the middle point. In order to produce maximum torque, the inverter must be commutated every 60° electrical angle. Therefore the micromotor need change 6 steps rotating 360° in an electrical angle, while 24 steps in mechanical 360°, shown in Fig. 14(b). Micromotors can be used as stepper motors with these two approaches. However, the accuracy is not high enough for the mission in micro fields, such as micromanipulation. 2-3 phases conducted approach (2-3 PCA), whose vector figure is shown in Fig. 14(c), can only increase the step accuracy of micromotors by two, which still limit applications of micromotors. Therefore, two novel approaches, Virtual-Winding Approach (VWA) and PWM (pulse width modulation) Based Vector-Synthesize Approach (PBVSA) are designed to improve the output torque and positional accuracy of electromagnetic synchronous micromotors without changing their structure. Both approaches are designed to control the value and direction of the current in each phase, then to change value and direction of synthetical magnetic, therefore to increase the steps of micromotor in 360° by electrical angle.

4.1 Virtual-Winding approach (VWA)

The VWA is realized by connecting the central point of the phases with a virtual winding, denoted as R', controlled by PWM signal, shown in Fig. 15. Through changing the frequency of the PWM pulse, the average value of the virtual winding is selected to change the current value of each phase. In VWA step control, the current through phase A, B, C and R' are denoted respectively as i1, i2, i3 and i', shown in Fig. 15. Where the R' is inserted into the circuit conducted as $A\overline{B}$ by parallel connection with phase A, expressed as $xA\overline{B}$. x represents the pulse duty cycle of the control PWM. The torque vector is shown in Fig. 16. If the steps required are fixed, then x is a fixed value which can be computed, and the torque value will also be a fixed value.

In this approach, 72 steps in 360° by mechanical angle are realized by inserting two steps into one step in 2-2 PCA. Then the communication phases sequence is:

$A\overline{C} \rightarrow xA\overline{C} \rightarrow xB\overline{C} \rightarrow B\overline{C} \rightarrow Bx\overline{C} \rightarrow \overline{x}AB \rightarrow \overline{A}B \rightarrow \overline{A}xB \rightarrow \overline{A}xC \rightarrow \overline{A}C \rightarrow \overline{x}AC \rightarrow \overline{x}BC \rightarrow \overline{B}C \rightarrow \overline{B}xC \rightarrow xA\overline{B} \rightarrow A\overline{B} \rightarrow Ax\overline{B} \rightarrow Ax\overline{C} \rightarrow A\overline{C}$

Compared with 2-2 PCA, there are 2 new steps with the VWA in a control step, which means 60° in electrical angle, shown in Fig. 15. According to law of sines, the expression can be drawn from Fig. 16.

$$\frac{i2}{i1} = \frac{\sin 50°}{\sin 10°} = \frac{1+x}{x} \tag{21}$$

Therefore,

$$x = 0.293 \tag{22}$$

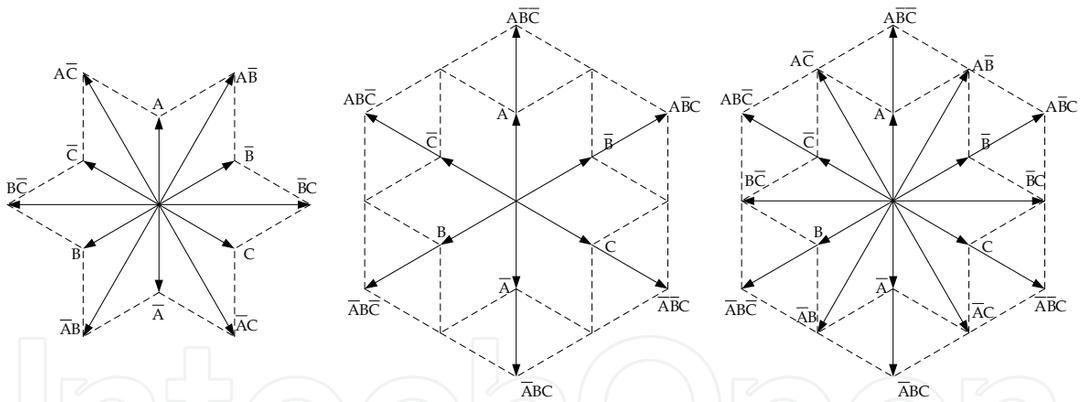

(a) 2-2 PCA control (b) 3-3 PCA control (c) 2-3 PCA control

Fig. 14. Vectors in an electrical angles 360°.

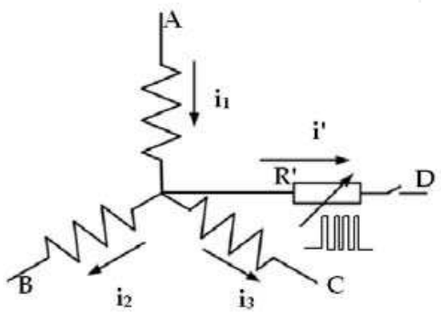

Fig. 15. Virtual winding principle for current divided.

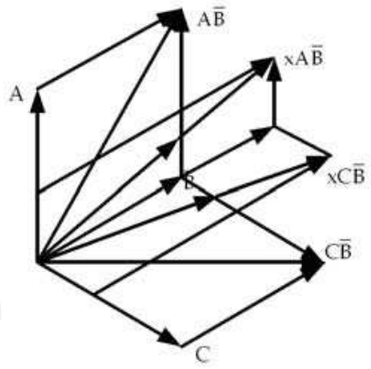

Fig. 16. Virtual winding control for step precision increasing.

Fig. 17 shows the experiment waves with the micromotor under 2-2 PCA control and virtual winding control. The black bumps in Fig. 17(b) are the voltage wave of the inserted steps. In theory, higher accuracy can be achieved in this approach by adding one extra PWM signal to the virtual winding. However, the virtual winding will reduce the output torque, incapable of providing constant torque output. This will weaken the performance of micromotors and applications will be limited as well.

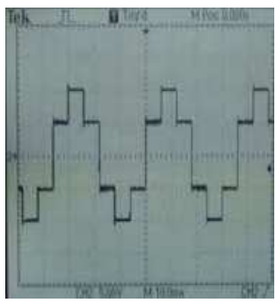

(a) 2-2 PCA control

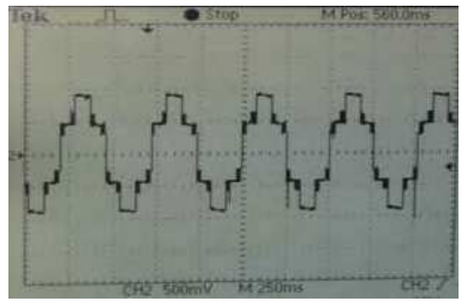

(b) Virtual coil control

Fig. 17. Voltage waveform of micromotor under 2-2 PCA control and VWA control.

4.2 PWM-Based-Vector-Synthesize approach (PBVSA)

PBVSA produces microstepping with a constant torque output for a micromotor, by utilizing the third coil in the three star-connected windings to divide currents into two parts, to synthesize the magnetic field, and to insert required steps.

PBVSA is based on the theory of torque vector synthesis. In 2-3 PCA control, when the stator is conducted with the current of $\bar{A}C$ at this time, the rotor will stop at its position. Then the stator will be conducted with the current of $\bar{A}\bar{B}C$, and the rotor will stop at a position with a 30°deviation in electrical angle. When two circuits are conducted alternately by two PWM signals, with one high frequency, the synthesis torque can be controlled by changing the ratio of these two currents, the stop position of the rotor is then decided. The frequency of PWM signal is at least ten times as much as that of commutation. Where the period of the PWM1 and PWM2 signals are t, t0 respectively, and t1 represents the conducted time of the two signals, the current through winding A (I_A) can be divided into two parts I_{A2} and I_{A3}, representing the currents when the stator is conducted as $\bar{A}C$ and $\bar{A}\bar{B}C$, respectively. As such the current IC can be divided into I_{C2} and I_{C3}. Their time sequence has been shown in Fig. 18. ince the two circuits cannot be conducted simultaneously, then:

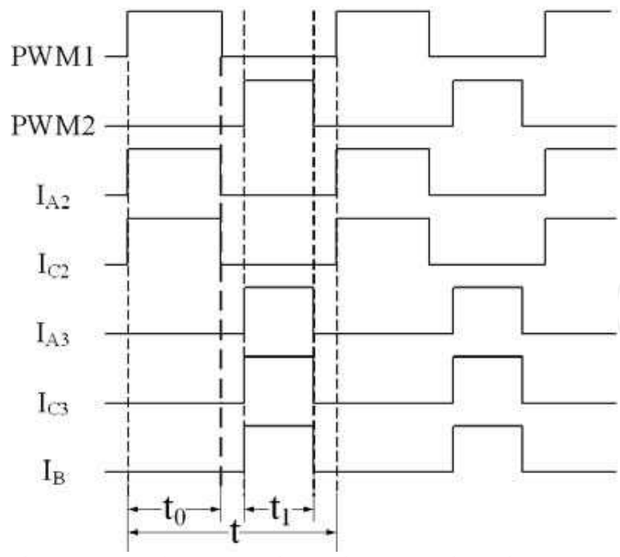

Fig. 18. Time sequence between PWM signals and every phase's current.

$$t > t_0 + t_1 \tag{23}$$

Assuming the resistance of each phase winding is R, the stator is conducted with a voltage of U, and the average value of I_{C3} in a period is:

$$\bar{I}_{C3} = \frac{t_1 \frac{2U_s}{3R} + 0}{t} = \beta I \tag{24}$$

Assuming β is pulse duty cycle of PWM2, and $\beta = t_1/t$. I is the rated current, $I = \frac{2U_s}{3R}$.

Similarly, the average value of I_{C2} in a period is:

$$\bar{I}_{C2} = \frac{t_0 \frac{U_s}{2R} + 0}{t} = \alpha \frac{3I}{4} \tag{25}$$

Assuming α is pulse duty cycle of PWM1, and $\alpha = t0/t$.
Therefore the average value of I_{A3} in a period is:

$$\bar{I}_{A3} = \frac{t_1 \frac{U_s}{3R} + 0}{t} = \beta \frac{I}{2} \tag{26}$$

and the average value of I_{A2} in a period is:

$$\bar{I}_{A2} = \bar{I}_{C2} = \alpha \frac{3I}{4} \tag{27}$$

while the average value of I_B is :

$$\bar{I}_B = \frac{t_1 \frac{U_s}{3R} + 0}{t} = \beta \frac{I}{2} \tag{28}$$

Since the magnetic field of the 2mm micromotor is designed with a trapezoid shape distributed in the gap between the stator and rotor, the average torque produced by I_{A2} and I_{C2} can be expressed as:

.

$$\bar{T}_2 = BL\sqrt{3}\alpha\frac{3I}{4}\frac{r}{2} = \alpha T \tag{29}$$

Where: B is the intensity in magnetic field between the rotor and stator; L is the valid length of each phase winding; r the average radius of the windings; $T = BL\sqrt{3}\frac{U_s}{2R}\frac{r}{2}$ is the largest value of the torque output under 2-2 PCA control. Under 3-3 PCA control, the average torque produced by I_{A3}、I_{B3} and I_{C3} is:

$$\bar{T}_3 = \frac{2\sqrt{3}}{3}\beta T \tag{30}$$

The vector relationship among $\bar{T}_M$, $\bar{T}_2$ and $\bar{T}_3$ must be kept as shown in Fig. 19. According to the law of cosines,

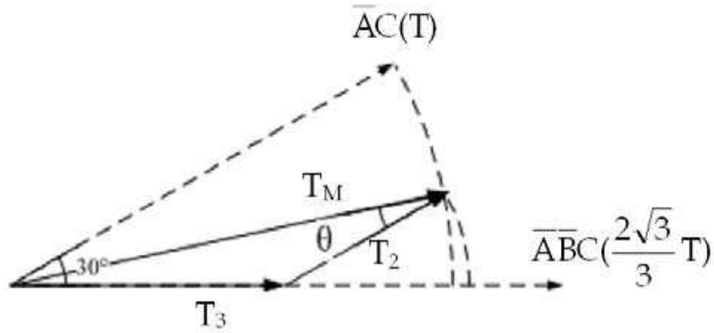

Fig. 19. Vector relation among $\bar{T}_M$, $\bar{T}_2$ and $\bar{T}_3$ while the synthesis torque is a constant.

$$T_M = \sqrt{\alpha^2 + (\frac{2\sqrt{3}}{3}\beta)^2 - 2\alpha\frac{2\sqrt{3}}{3}\beta\cos(\frac{5\pi}{6})} \tag{31}$$

Therefore, the synthesis torque output is not decided by the required steps, which means a constant torque output can be obtained by PBVSA.

To get T_M with the constant value of T, the following constraints must be obtained according to law of sine:

$$\alpha = \frac{\sin(\frac{\pi}{6} - \theta)}{\sin\frac{5\pi}{6}} = 2\sin(\frac{\pi}{6} - \theta) \tag{32}$$

$$\beta = \frac{\sqrt{3}}{2}\frac{\sin\theta}{\sin\frac{5\pi}{6}} = \sqrt{3}\sin\theta \tag{33}$$

Thus, the microstepping with constant torque output for an electromagnetic micromotor can be obtained by changing the values of α and β.

Microstepping with constant torque for a star-connected PM micromotor is realized without any additional circuit to change the value, which will result in a higher efficiency compared with VWA. However, this method requires a more complicated control circuit to produce the time sequences. At present, experiments of 144 steps in 360° by mechanical angle have been obtained under PBVSA control. The control waves, the phase voltage changing relatively to the ground, and the amplified part, are shown in Fig. 20(a) and Fig.

20(b).

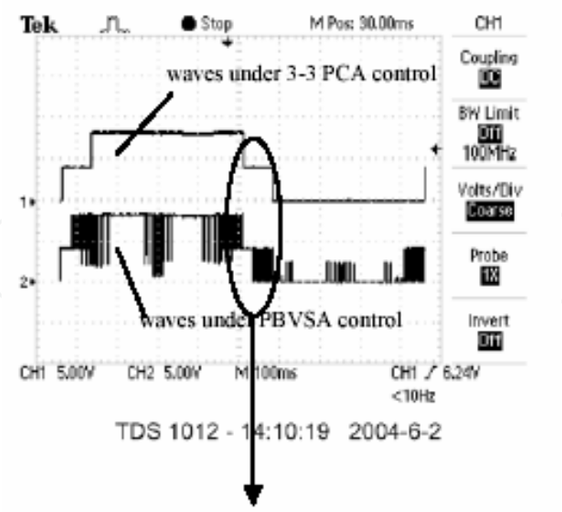

(a) Waves in one commutating period

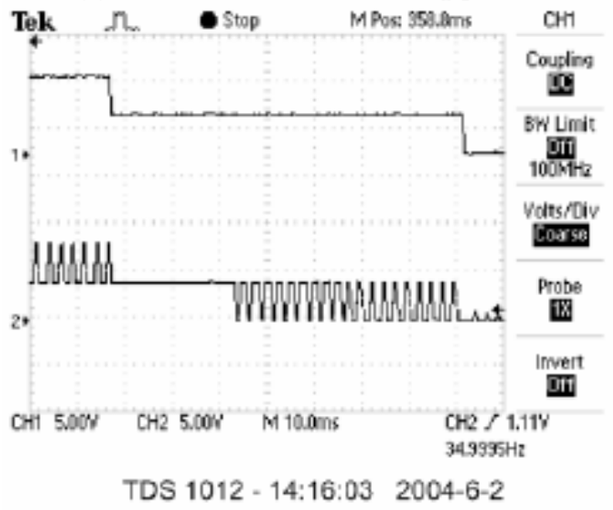

(b) Amplified waves

Fig. 20. Waves of voltage between coil conducted and ground under 3-3 PCA control and PBVSA control.

The statistical data of the deviation angle, obtained from the real position and the designed angle during a 360 mechanical angle in the experiment, is shown as Table 2. The deviation is led by the uneven magnetic field intensity at the edges of the magnetic poles.

Both Virtual-Winding Approach (VWA) and PWM Based Vector-Synthesize Approach (PBVSA) are designed to realize the microstepping of microrobots without changing the present structure of micromotors. These are limited by the present microfabrication process, and to explore the new applications for electromagnetic micromotors. Though these novel approaches are demonstrated by the 2mm micromotor, they can be applied for the electromagnetic micromotors with similar structures like PM motors, with either axial or radial direction magnetic field.

Deviation angle	0~0.2°	0.2~0.3°	0.3~0.5°
Number of steps	75	36	33

Table 2. Test result of the micromotor under PBVSA control.

5. Application of the omni-directional microrobot

The omni-directional microrobots within 1cm^3 (shown in Fig. 21), were designed for microassembly in narrow space, and have been applied into a microassembly system, to manipulate and transport a microbearing with a 0.6mm inner diameter and a 1mm outer diameter, and to assemble it in an axis with 0.4mm diameter. The system is composed of omni-directional microrobots with a microgripper, an assembly platform, a visual system and a microrobots controller (shown in Fig. 22). The assembly platform is divided into an assembly part and a transport part. The visual system consists of three CCD cameras, a visual grabber card, and a computer. One normal CCD camera covers the whole platform as the global visual sensor, while the other microscope CCD cameras cover the assembly parts as the local sensor. The acquisition and tracking algorithm is run to acquire the positions and postures of the microrobots. The controller decides the microrobots behaviour by communicating with the visual system to execute the assembly mission.

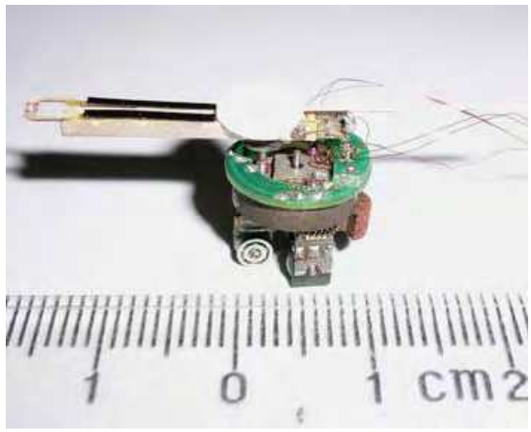

Fig. 21. Photo of the microrobot with micro gripper.

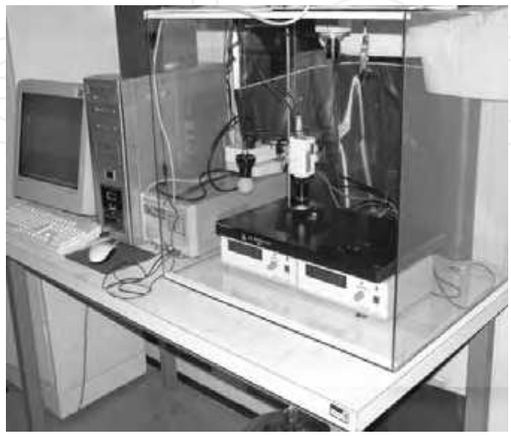

Fig. 22. Photo of the micro assembly system.

The microrobot is capable of moving continuously or in stages with a high precision. Both of the two novel approaches, VWA and PBVBA, are applied into this microrobot. The results are showed in the following Table 3.

	VWA	PBVSA
Translation precision	0.11mm/Step	0.04mm/Step
Rotation precision	1.25°/Step	0.625°/Step

Table 3. Contrast results between two methods applied on a microrobot.

Table 3 shows that PBVSA can achieve higher precision than VWA under the same controlling circumstances. It is because in the VWA approach, a resistor is used and thereby consumes part of the power. However, its simpler circuit make VWA easy to produce.

6. Conclusion

This chapter has presented the construction of an omni-directional mobile microrobot system, with the microrobot less than one cubic centimeter in volume and its unique dual-wheels driven by electromagnetic micromotors, two millimeters in diameter, for purpose of microassembly in narrow space. The results show that the microrobot can move continuously or in stages with high precision under the two novel micro step control approaches, which is necessary for the microassembly mission. This omni-directional mobility and the high precision movement show that the omni-directional mobile microrobot will have many potential applications in micro fields.

Although this work shows a good performance of a microrobot, there is still some further work needed for this microrobot as the precision of the microbot is not enough for the nano-manipulation and the power consumption of the microrobot is not very satisfying. In order to accomplish more complex work, the multiple microrobots cooperation control still needs to be adopted.

7. References

Alexander, J.C. & Maddocks, J.H. (1989) On the Kinematics of Wheeled Mobile Robots. *Int. Journal of Robotics Research*, Vol. 8, No. 5, (Aug. 1989) 15-27

Brufau, J.; Puig-Vidal M.; et al. (2005). MICRON: Small Autonomous Robot for Cell Manipulation Applications, *Proc. of the IEEE International Conference on Robotics & Automation,* pp. 856-861, Barcelona, Spain, April, 2005

Boreinstein , J.; Everett, H.R. & Feng, L. (1996). *Navigating Mobile Robot*. AK Peters, Wellesley, Massachusetts

Byrne, R.H.; Adkins, D.R.; Eskridge, S.E.; Harrington, J.J.; Heller, E.J. & Hurtado J.E. (2002). Miniature Mobile Robots for Plume Tracking and Source Localization research. *Journal of Micromechatronics*, Vol. 1, No. 3, (2002) 253-260

Caprari, G.; Balmer P.; Piguet, R. & Siegwart, R. (1998). The Autonomous Micro Robot ALICE: A Platform for Scientific and Commercial Applications, *MHS'98*, pp. 231-235, Japan, 1998

Dario, P. ; Carrozza, MC ; Stefanini, C. & D'Attanasio, S. (1998). A Mobile Microrobot Actuated by a New Electromagnetic Wobble Micromotor. *IEEE/ASME Transactions on Mechatronics*, Vol. 3, No. 1, (1998) 9-16

Fearing, R.S. (1997). Micro-Actuators for Micro-Robots: Electric and Magnetic, Tutorial Su 1: Micro Mechatronics, *IEEE1997 Int. Conf. on Robotics and Automation*, Albuquerque, NM April 20, 1997

Ferriere, L. & Raucent, B. (1998). ROLLMOBS, a New Universal Wheel Concept, *Proceedings of IEEE International Conference on Robotics and Automation,* pp.1877-1882, Leuven, Belgium, 1998

Fujisawa, S.; Ohkubo, K.; Yoshida, T.; Satonaka, N.; Shidama, Y. & Yamaura, H. (1997). Improved Moving Properties of An Omnidirectional Vehicle Using Stepping Motor, *Proceedings of the 36th Conference on Decision & Control*, pp. 3654-3657, San Diego, California,1997

Killough, S.M. & Pin, F.G. (1994). A New Family of Omnidirectional and Holonomic wheeled platforms for mobile robots. *IEEE Transactions on Robotics and Automation*, Vol. 10, No. 4, (1994) 480-489

Kim,D.; Kwon, W. H. & Park H. S. (2003). Geometric Kinematics and Applications of a Mobile Robot. *International Journal of Control, Automation, and Systems,* Vol. 1, No. 3, (Sep. 2003) 376-384

Li, Z. & Zhang C. (2000). Genetic Algorithms for the Optimal Design of Electromagnetic Micro Motors, *High Technology Letter*, Vol.6, No.1, (2000) 50-54

Mclurkin, J. (1996). *Using Cooperative Robots for Explosive Ordonance Disposal*, MIT AILab, 1996

Muir, P.F. & Neuman, C.P. (1987). Kinematic Modeling for Feedback Control of an Omni-directional Wheeled Mobile Robot, *Proceedings of IEEE International Conference on Robotics and Automation*, pp. 1772-1778, Raleigh, N.C. USA, March 1987

Schmoeckel F. & Fatikow, S. (2000). Smart Flexible Microrobots for Scanning Electron Microscope (SEM) Applications. *Journal of Intelligent Material Systems and Structures,* Vol. 11, No. 3, (2000)191-198

Thorbjörn, E.; Johan, U. M.; Edvard K. & Göran S. (1999). Walking Silicon Micro-robot, *The 10th Int Conference on Solid-State Sensors and Actuators (Transducers'99)*, pp 1202-1205, Sendai, Japan, June 7-10, 1999

Vartholomeos P. & Papadopoulos E. (2006). Analysis, Design and Control of a Planar Micro-robot Driven by Two Centripetal-Force Actuators, Proceedings of the 2006 IEEE International Conference on Robotics and Automation, pp. 649-654, Orlando, Florida, USA, May 2006

Williams, R. L.; Carter, B. E.; Gallina, P & Rosati, G. (2002). Dynamic Model with Slip for Wheeled Omnidirectional Robots. *IEEE Transactions on Robotics and Automation*, Vol. 18, No. 3, (June 2002) 285-293

West, M. & Asada, H. (1997). Design of Ball wheel Mechanisms for Omnidirectional Vehicles With Full Mobility and Invariant Kinematics. *Journal of Mechanical Design*, Vol.119, (1997) 153-161

Wada, M., & Mori, S. (1996). Holonomic and Omnidirectional Vehicle with Conventional Tires, *Proceedings of IEEE International Conference on Robotics and Automation*, pp. 3671-3676, Minnesota, USA, 1996

Zhao, X.; Yang,C.; Ding, G.& Zhang M. (1999). Fabrication of Stator Winding of Electromagnetic Micromotor with 1mm Diameter, Proc. SPIE Electronics and Structures for MEMS, Vol. 3891, pp. 352-358, October 1999, Royal Pines Resort, Queensland, Australia, Sep. 1999

Mobile Robots: towards New Applications

Edited by Aleksandar Lazinica

ISBN 978-3-86611-314-5

Hard cover, 600 pages

Publisher I-Tech Education and Publishing

Published online 01, December, 2006

Published in print edition December, 2006

The range of potential applications for mobile robots is enormous. It includes agricultural robotics applications, routine material transport in factories, warehouses, office buildings and hospitals, indoor and outdoor security patrols, inventory verification, hazardous material handling, hazardous site cleanup, underwater applications, and numerous military applications. This book is the result of inspirations and contributions from many researchers worldwide. It presents a collection of wide range research results of robotics scientific community. Various aspects of current research in new robotics research areas and disciplines are explored and discussed. It is divided in three main parts covering different research areas: Humanoid Robots, Human-Robot Interaction, and Special Applications. We hope that you will find a lot of useful information in this book, which will help you in performing your research or fire your interests to start performing research in some of the cutting edge research fields mentioned in the book.

How to reference

In order to correctly reference this scholarly work, feel free to copy and paste the following:

Zhenbo Li and Jiapin Chen (2006). Omni-directional Mobile Microrobots on a Millimeter Scale for a Microassembly System, Mobile Robots: towards New Applications, Aleksandar Lazinica (Ed.), ISBN: 978-3-86611-314-5, InTech, Available from: http://www.intechopen.com/books/mobile_robots_towards_new_applications/omni-directional_mobile_microrobots_on_a_millimeter_scale_for_a_microassembly_system

INTECH
open science | open minds

InTech Europe
University Campus STeP Ri
Slavka Krautzeka 83/A
51000 Rijeka, Croatia
Phone: +385 (51) 770 447
Fax: +385 (51) 686 166
www.intechopen.com

InTech China
Unit 405, Office Block, Hotel Equatorial Shanghai
No.65, Yan An Road (West), Shanghai, 200040, China
中国上海市延安西路65号上海国际贵都大饭店办公楼405单元
Phone: +86-21-62489820
Fax: +86-21-62489821

IntechOpen